Hindawi
Advances in Materials Science and Engineering
Volume 2019, Article ID 2878060, 9 pages
https://doi.org/10.1155/2019/2878060

Research Article

NaI Doping Effect on Photophysical Properties of Organic-Lead-Halide Perovskite Thin Films by Using Solution Process

Chuangchuang Chang, Xiaoping Zou, Jin Cheng, Ying Yang, Yujun Yao, Tao Ling, and Haiyan Ren

Beijing Advanced Innovation Center for Materials Genome Engineering, Research Center for Sensor Technology, Beijing Key Laboratory for Sensor, MOE Key Laboratory for Modern Measurement and Control Technology, School of Applied Sciences, Beijing Information Science and Technology University, Jianxiangqiao Campus, Beijing 100101, China

Correspondence should be addressed to Xiaoping Zou; xpzou2014@163.com

Received 1 February 2019; Revised 26 March 2019; Accepted 1 April 2019; Published 3 June 2019

Guest Editor: Zeyun Xiao

Perovskite solar cells (PSCs) have been developed rapidly in recent years. How to modify the photophysical properties of perovskite films has become the critical issue, affecting device performance. In this paper, NaI doping into the perovskite layer is attempted to modulate the photophysical properties to improve the performance of PSCs. The perovskite layer was prepared by using the one-step solution spin coating method with doping different concentrations of NaI into the perovskite precursor solution and chlorobenzene employed as the antisolvent. Experimental results show that the absorption band edge and the peak position of the PL spectrum of the doped perovskite thin film were red shifted; thus, the band gap of the semiconductor film became narrow. Doping NaI into perovskite is an effective way, by which the photophysical properties of perovskite films are well modified, thus improving device performance.

1. Introduction

In recent years, with the rapid development of photovoltaic industry, PSCs are considered the most potential for the future of the new type of solar cells because the advantages of low cost, simple preparation and high efficiency make it the first choice to replace the traditional crystalline silicon solar cell [1–7]. In the preparation of batteries, the morphology of perovskite layers [8–12] (including grain size, grain boundary direction, effective film thickness, pore cracks, and surface flatness) and photophysical properties [13–15] (including band edge displacement, band gap, carrier mobility, and lifetime [16]) are critical to the performance of devices. If there are cracks and pinholes in the perovskite layer, the light absorption rate will be reduced, the photocurrent will be reduced, and the internal resistance of the battery will be increased. Moreover, it can lead to the contact between the electron transport layer and the hole transport layer, intensify the composite of perovskite photocarriers, increase the leakage current, and thus reduce the performance of the perovskite solar cell. Therefore, it is necessary to study how to prepare thin films with good morphology and optical semiconductor properties.

The earliest study of Na^+ doping was experimentally used for preparation of Cu(In, Ga)Se_2 (CIGS) solar cells. In 2000, Granath's team doped Na^+ into the absorption layer film to improve the performance of CIGS solar cell devices [17]. In 2009, Caballero et al. studied the effect of Na^+ on the electronic properties and structure of the CIGS absorption layer [18]. In 2016, according to the theory of the first principle, Yuan et al. found that Na diffusion enhanced p-type conductivity in Cu(In, Ga)Se_2 [19]. It has been reported that rubidium-doped [20] and cesium-doped [21] PSCs have better stability and higher power conversion efficiency

(PCE) than pure PSCs. Hong et al., trying to study the advantages of perovskite as a light-absorbing layer material, found that this material can tolerate some internal defects and the intrinsic perovskite material can be self-doped using defect engineering [22, 23]. Mojtaba abdi-jalebi et al. found that Na^+, Cu^+, and Ag^+ cationic halides have ionic radii similar to Pb^{2+} and can be doped into the perovskite absorption layer to regulate the morphology and photophysical properties of perovskite to improve the photovoltaic performance of perovskite thin films [24].

A challenging issue in the preparation of PSCs is that nonradiative recombination of electrons and holes will occur during the transmission process, resulting in loss of photocarriers and reduced cell efficiency and performance. If the separation and extraction speed of carriers in the perovskite layer is accelerated, the nonradiative recombination of internal carriers will be reduced. It is envisaged that, on the basis of these studies, the majority of perovskite carrier properties will be changed via experiments, and the perovskite layer will be made into the p-n junction. Under the action of the internal built electric field, the separation and extraction speed of carriers will be improved a lot, and the probability of nonradiation recombination will be reduced a lot, so the performance of the device will be improved. This paper attempts to dope Na^+ into the perovskite layer to modulate the morphology and photophysical properties of the light absorption layer and improve the performance of PSCs.

At present, the certification efficiency of experimental samples exceeds 20%, and the majority of them use metal as the counter electrode (gold and silver) [25, 26]. This will undoubtedly increase the cost of device preparation, which is not conducive to the commercial production of PSCs. Some researchers use the carbon film, greatly reducing the production cost. Yang et al. prepared a perovskite solar cell with an efficiency of 2.6% by using candle soot carbon as the counter electrode [27]. In our research group, discussed with doping Na^+ of low concentration on the morphology and physical properties of the device [28], sponge carbon was used as the electrode, and PCE [29] reached 4.24%. Recently, the effect of crystallization rate on grain size after solution treatment was described [30], the PSCs prepared by sequential deposition method and the carbon film were used as the counter electrode, and PCE [31] reached 10.7%.

Existing anion-doped elements mainly include Cl^-, while cation-doped elements mainly include Na^+, K^+, Rb^+, Cs^+, and other alkali metal ions. The perovskite layer was prepared by using the one-step solution spin coating method with doping different concentrations of NaI into the perovskite precursor solution and chlorobenzene employed as the antisolvent [32]. It can be seen from the SEM that the doped perovskite film has larger grain size, higher thickness, and fewer grain boundaries and holes. It can be seen from the UV-visible absorption spectrum that its absorption characteristics become better, and both the absorption spectrum and PL spectrum show red shift [7] compared with the pure $MAPbI_3$. In normal temperature, PSCs were prepared by the one-step solvent method and the carbon film, with a PCE value of 7.62% and an area of 0.12 cm^2.

2. Materials and Experimental Methods

2.1. Materials. The FTO conductive glass is the transparent conductive SnO_2 glass doped with fluorine as the substrate of the thin film solar cell, purchased from Shanghai MaterWin New Materials Co., Ltd (Shanghai, China). Dimethyl sulfoxide (DMSO) and N,N-dimethyl formamide (DMF) were purchased from Alfa Aesar (China) Co., Ltd (Shanghai, China). Acid titanium dioxide solution (bl-TiO_2) and 18NR-T TiO_2 (mp-TiO_2), isopropanol (IPA), and chlorobenzene were purchased from Shanghai MaterWin New Materials Co., Ltd (Shanghai, China). Spiro-OMeTAD solution, methylammonium iodide (MAI), PbI_2, and NaI were obtained from Xi'an Polymer Light Technology Corp (Xi'an China).

2.2. Device Fabrication. The overall structure of the device is FTO/bl-TiO_2/mp-TiO_2/$CH_3NH_3PbI_3$/Spiro/FTO(C) from bottom to top. The FTO conductive glass is a photoanode material for solar cell devices, which must be cleaned before use. After cutting the glass, ultrasonic cleaning of FTO was carried out successively with mixed solution (detergent and deionized water), glass water (acetone : deionized water : 2-propanol = 1 : 1 : 1), and alcohol. After washing with deionized water and drying for 30 minutes, the FTO was ozone-treated with ultraviolet ozone (UVO) for one hour before use. The TiO_2 compact layer (bl-TiO_2) was spin-coated with a layer of acidic TiO_x solution at a rate of 2000 rpm for 60 s and then on the hot plate heated to 100°C for 10 min. Finally, in the muffle furnace, 30 minutes under 500°C, calcination will give a smooth highly dense TiO_2 layer. The TiO_2 mesoporous layer (mp-TiO_2) was spin-coated with a layer of the 18NR-T TiO_2 slurry solution at 2000 rpm for 30 s, afterward on the hot plate heated to 100°C for 10 min, and finally in the muffle furnace under 500°C calcination and 1 hour to get an uniform mesoporous TiO_2 layer.

Two kinds of precursor MAI ($CH_3NH_3PbI_3$) and PbI_2 (concentrations were 1.2 mol/L and 1.3 mol/L) were dissolved in dimethyl sulfoxide (DMSO) and N, N-dimethylformamide (DMF) of two kinds of solvents (volume ratio of 1:4) in the mixed solution. Masses 0.1125 g, 0.135, and 0.18 g NaI were dissolved in the well-prepared precursor solution. After that, 0.75 mol/L, 0.9 mol/L, and 1.2 mol/L of yellow transparent doped NaI perovskite precursor solution could be obtained. After the solution was allowed to stand for 12 hours, it was filtered to obtain very clear doped $MAPbI_3$ precursor solution. Two stages are required for perovskite coating: 1000 rpm for 10 s and 3000 rpm for 30 s. 20 ul of chlorobenzene was added with 15 s left in the second stage. On the hot plate, under 100°C annealing 40 min, perovskite film or the film doped into perovskite can be obtained. An appropriate amount of Spiro spin coating to the perovskite film was applied. The hole transport layer is obtained by rotating it for 30 s at the rate of 3000 rpm. Finally, the counter electrode was cleaned with FTO as the substrate, and the smoke particles generated by candle combustion formed the carbon film. The prepared carbon

film was aligned on the top layer of the prepared device. A small clip was used to clamp the sides for easy packaging.

2.3. Characterization. The morphology of the perovskite films was measured using a scanning electron microscope (SEM) (SIGMA, Zeiss, Jena, Germany). The equipment can also test energy dispersive X-ray spectroscopy (EDS) for chemical composition analysis of doped perovskite film samples. X-ray diffraction (XRD) data from samples of perovskite films deposited onto FTO/bl-TiO_2/mp-TiO_2 substrates were collected using an X-ray diffractometer (D8 Focus, Bruker, Dresden, Germany). The absorption spectra of perovskite films with different doping concentrations of K^+ were analyzed by an ultraviolet (UV) visible absorption spectrometer (Avantes, Apeldoom, The Netherlands), and the PL was examined by a LabRAW HR800 PL testing system (HORIBA JObin Yvon, Paris, France). Photocurrent density-voltage (J-V) characteristics were measured under simulated standard air quality daylight (AM 1.5, 100 mW/cm^2) with using a solar simulator (Sol 3A, Oriel, Newport, RI, USA).

3. Results and Discussion

0 M, 0.75 M, 0.9 M, and 1.2 M·NaI solids were dissolved in 1 ml of the prepared perovskite solution, named Sample+0 M, Sample+0.75 M, Sample+0.9 M, and Sample+1.2 M, respectively. Different doping concentrations of perovskite membrane top view and cross section diagram of SEM images are shown in Figure 1, and it can clearly be seen that they modulate the topography of the surface of the perovskite film by controlling the concentration of doped Na^+.

Figures 1(a), 1(c), 1(e), and 1(g) are SEM images showing the top views of perovskite thin films prepared with the NaI-doped perovskite solution with zero doping and different concentrations, respectively. Figures 1(b), 1(d), 1(f), and 1(h) are SEM images showing the cross section of perovskite thin films prepared with zero doping and different concentrations of the NaI-doped perovskite solution, respectively. Magnification is 20,000 times. It can be seen from Figure 1 that the three kinds of perovskite film particles prepared by doping are very large. However, Figures 1(e) and 1(g) show cracks and obvious grain boundaries because perovskites are exposed to the air. The results show the formation of the $MAPbI_3{\cdot}H_2O$ intermediate with water molecules in the air, thus inevitably leading to the breakdown of perovskite films. It can be found in the SEM images that when the dope concentration is 1.2 mol/L, a minor change occurs in the morphology of the perovskite films, which produces square particles.

Comparing Figure 1(c) with Figure 1(e), Figure 1(c) shows relatively more surface cracks, and the overall surface of the perovskite layer is not smooth enough, with many bumps. In Figure 1(d), it is apparent that there are different directions and irregular grain boundaries, and there are still small holes in the perovskite layer. For the carrier to the electronic transport layer and hole transport layer separation, transmission has a certain impact. This is why the efficiency of the Sample+0.75 M perovskite solar cell device is worse than Sample+0.9 M. Due to excessive grain boundaries and large cracks exposed to air as shown in Figure 1(g), a $MAPbI_3{\cdot}H_2O$ intermediate is formed with water molecules in the air, which causes decomposition of the perovskite film [33].

As a result, the effective thickness of the perovskite film of Sample+1.2 M is relatively less. From the cross-sectional view shown in Figure 1(h), it can be seen that there is a distinct hole in the place where the mesoporous TiO_2 layer is contacted and the cracks between the blocks seem to be larger. There are many crystal boundaries between grains, and the perovskite layer has an obvious block-like structure and irregular crystal blocks. These boundaries and irregular crystal blocks will affect the separation and transmission of carriers to the electron transport layer and hole transport layer. This is also the reason why the efficiency of the perovskite solar cell device of Sample+1.2 M is worse than that of Sample+0.9 M.

Comparing Figure 1(h) with Figure 1(d), it can be seen that the grain boundaries in Figure 1(h) are obvious and the cracks are large, but they are all vertical grain boundaries with limited influence on carrier transport. However, there are irregular grain boundaries in different directions in Figure 1(d) and still small holes in the perovskite layer. It has a great influence on the separation of carrier over the electron transport layer and hole transport layer. As a result, the device efficiency of Sample+1.2 M is higher than that of Sample+0.75 M. The perovskite layers shown in Figures 1(d), 1(f), and 1(h) are of similar thickness, but the cross section of the perovskite layers shown in Figure 1(f) is generally more uniformly flat, and Figure 1(f) shows the perovskite layers have substantially negligible grain boundaries in the vertical direction. The carriers move along the vertical direction, and the decrease in the grain boundary is beneficial for the carriers to separate the electron transport layer and hole transport layer. The results showed that the Sample+0.9 M perovskite battery device had the best performance.

In addition, comparing with Figure 1(a), it can be found in the top view of Figures 1(c), 1(e), and 1(g) that the doped Na^+ forms a perovskite film with a smoother overall surface and fewer cracks between the crystal blocks. The size of doped perovskite crystal grains is about three times larger than that of undoped crystal grains; therefore, it can be said that the quality of the whole perovskite layer has been greatly improved. Comparing with Figure 1(b), it can be found in the cross-sectional view of Figures 1(d), 1(f), and 1(h) that the thickness of the perovskite film doped with Na^+ is much thicker than that of the undoped perovskite film. Compared with the pure perovskite films, the doped cross-section images have fewer pores and grain boundaries, forming more favorable conditions for carrier migration.

Furthermore, in order to verify whether Na^+ has been incorporated into the perovskite layer films of $MAPbI_3$, EDS elemental analysis results of perovskite layer films doped with Na^+ at different concentrations is given in Figure 2. The EDS of the samples shows that the perovskite microcrystalline film has Na^+. In EDS, we can see that the peak strength of sodium (shown in red circle) increases gradually

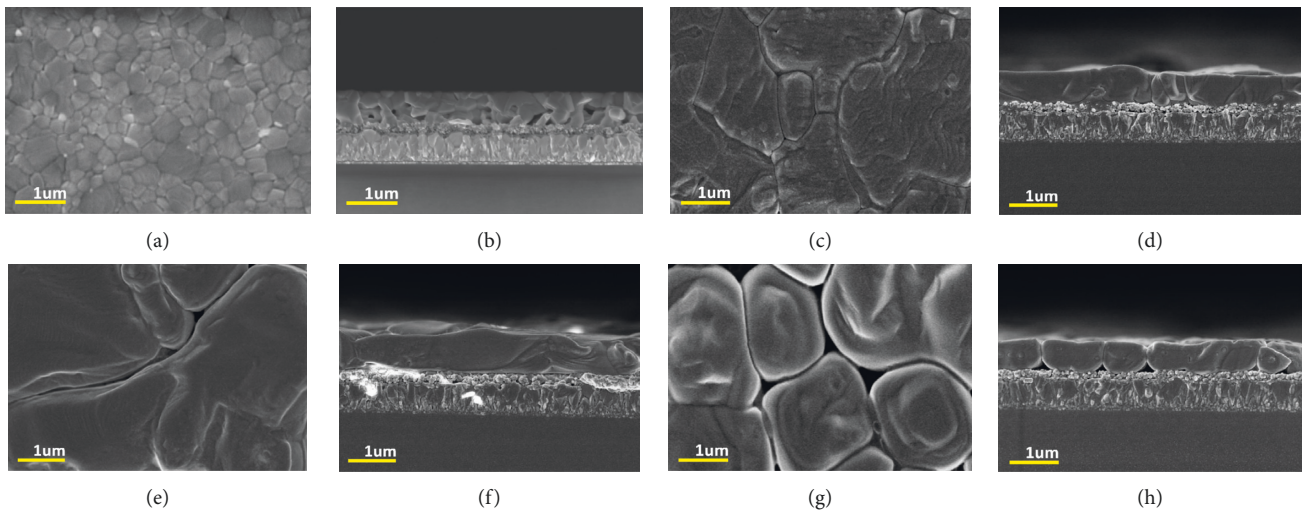

FIGURE 1: Top view and cross-sectional view of the SEM images for Sample+0 M (a, b), Sample+0.75 M (c, d), Sample+0.9 M (e, f), and Sample+1.2 M (g, h).

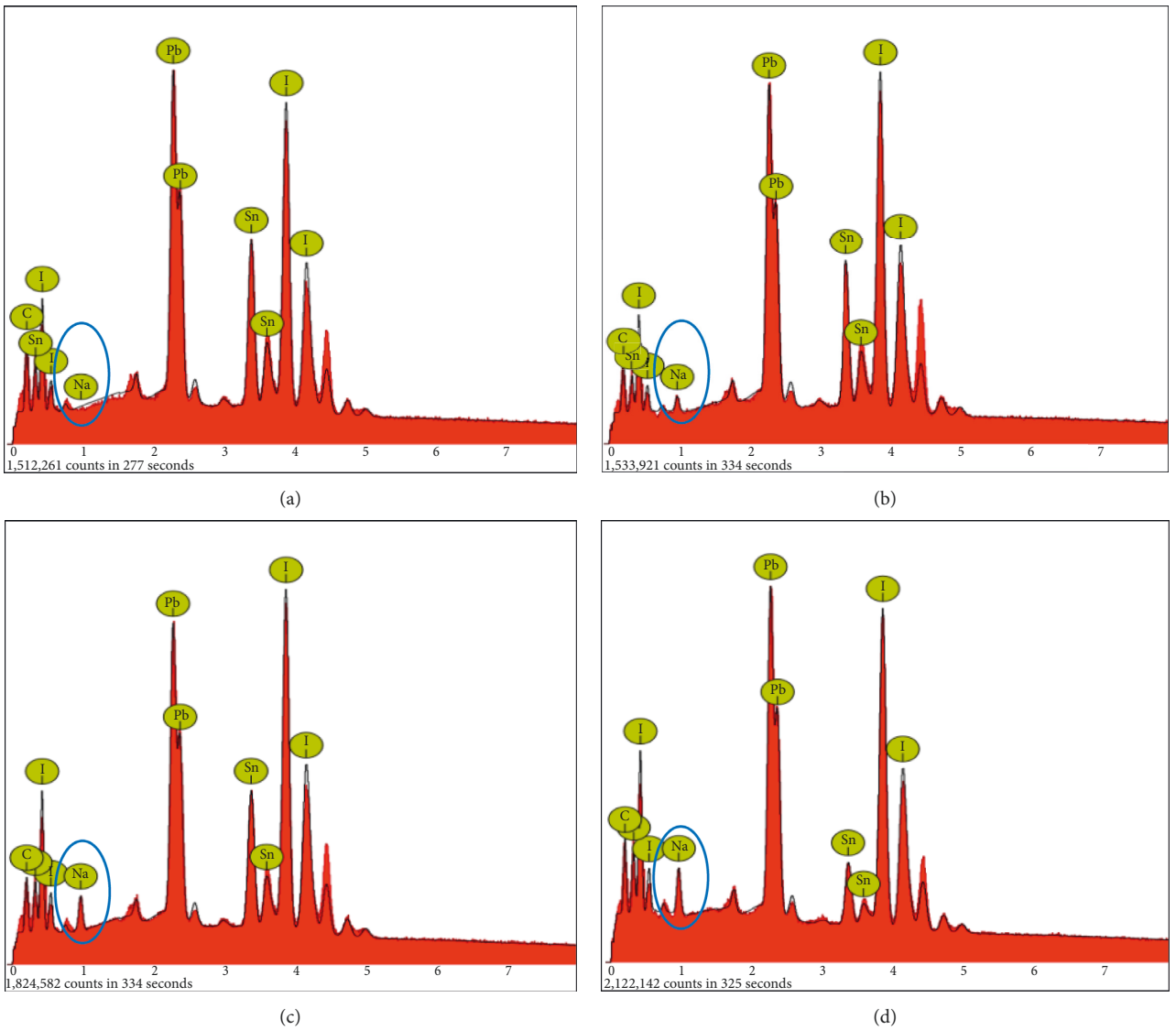

FIGURE 2: The energy dispersive X-ray spectroscopy (EDS) of films with Sample+0 M (a), Sample+0.75 M (b), Sample+0.9 M (c), and Sample+1.2 M (d) (the blue ellipse area is the peak position of Na^+).

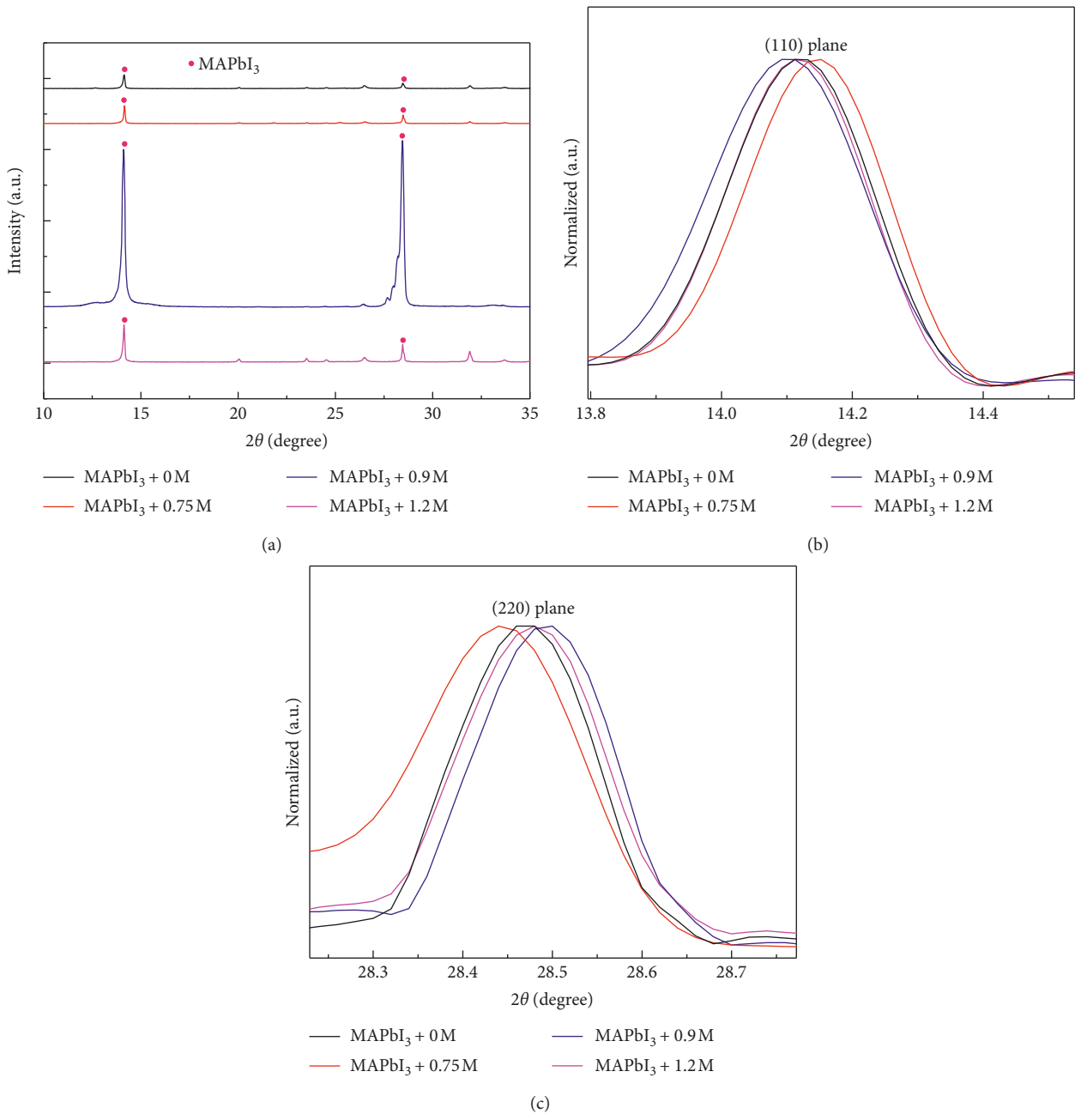

Figure 3: XRD patterns of perovskite films with Sample+0 M, Sample+0.75 M, Sample+0.9 M, and Sample+1.2 M: (a) whole patterns; (b) enlargement of (110) crystal plane; (c) enlargement of (220) plane.

with the increase in the doping concentration of sodium, and the signal strength becomes more and more obvious. From the SEM images, it can be found that, with the addition of sodium, the perovskite grains become larger and the thickness of the film increases significantly.

Figure 3 shows further observation of the effect of Na^+-doped perovskite solution on the crystal structure of perovskite. The XRD images of the four groups of devices show that the characteristic peaks of doped perovskite and pure $MAPbI_3$ appeared in $2\theta = 14.17$ and 28.24, corresponding to the crystal faces of the perovskite (110) and (220). From the XRD image (Figure 3(a)), it can be found that with the increase in doping concentration, the ratio of crystal face index (110) and crystal face index (220) characteristic peak intensity increase with the decrease of the first. Figures 3(b) and 3(c) show the curve of characteristic peaks after the normalized smoothing of crystal surface indices (110) and (220), respectively. Na^+ doping has an effect on the growth of the crystal surface, leading to the change of perovskite morphology. When doping Sample+0 M, Sample+0.75 M, and Sample+1.2 M, the ratio of characteristic peak strength is all greater than 1, and only when doping Sample+0.9 M, the ratio of characteristic peak strength is less than 1.

It can be concluded that when doped with Sample+0.9 M, the influence of Na^+-doped perovskite solution on the crystal structure of the perovskite layer is significantly different from that of the other three groups of samples. Here, we combine the SEM images of Figure 1 for observation, the SEM image of doping Sample+0.9 M is the one with the largest flatness, and the grain boundary in the cross-section image basically has no obvious holes or bumps. Therefore, it is speculated that the battery performance of doping Sample+0.9 M may be significantly different from other samples, and the battery performance may be better.

All perovskite films were prepared on FTO/bl-TiO_2/mp-TiO_2 substrates. It can be clearly seen from Figure 4 that the absorption range of pure $MAPbI_3$ perovskite film and the perovskite film prepared by NaI-doped perovskite solution is between 400 nm and 750 nm. The higher the Na^+ doping concentration, the more obvious the red shift of the absorption band edge of the perovskite film. In this paper, it is pointed out that the absorption band edge red shift in the absorption spectrum shows the positional change at the intersection of the absorption band edge extension line and the abscissa axis. In this paper, the red shift is due to the improvement of the crystallinity of perovskite after doping with Na^+, and crystal surface passivation enhances the crystal structure and film thickness, reduces defect density, and improves crystallization quality. The alkali metal cation Na^+ with small ion radius was added to modulate the band gap, band gap reduction. Finally, the UV-visible red shift occurred [7, 24, 34].

Figure 5 shows the various concentrations of Na^+-doped perovskite thin film photoluminescence spectrogram and shows that the samples are in the preparation of mesoporous TiO_2. It can be clearly seen from Figure 5 that the emission peak of $MAPbI_3$ perovskite appears around 770 nm. By comparison, the emission peaks of NaI-doped perovskite films all moved to a longer wavelength range. The results are consistent with references [7, 35]. Also, with the continuous increase in concentration of NaI, the PL peak position of long wavelength shift and the band gap narrows gradually. The top left corner of the graph is the normalized PL graph, and it can be clearly seen that the PL emission peak of the perovskite layer film after doping has red shifted, which is consistent with the conclusion of the corresponding absorption spectrum. Doping can regulate the photophysical properties of semiconductor perovskite thin film materials, which is expected to be used in solar cells.

The device structure prepared in this experiment is shown in Figure 6(a), FTO/bl-TiO_2/mp-TiO_2/$CH_3NH_3PbI_3$/Spiro/Carbon/FTO). The solar rays enter from the bottom and pass through the electron transport layer to the doped perovskite layer and then to the hole transport layer and the electrode prepared by the carbon film to form a loop. The J-V curve of the Na^+-doped perovskite solar cell device is shown in Figure 6(b), the device corresponding to the four performance parameters are shown in Table 1. From the detailed data in Table 1, it can also be seen that when the NaI doping concentration is 0.9 mol/L; the performance of PSCs is best; J_{sc}, V_{oc}, and FF are 18.11 mA/cm^2, 908 mV, and

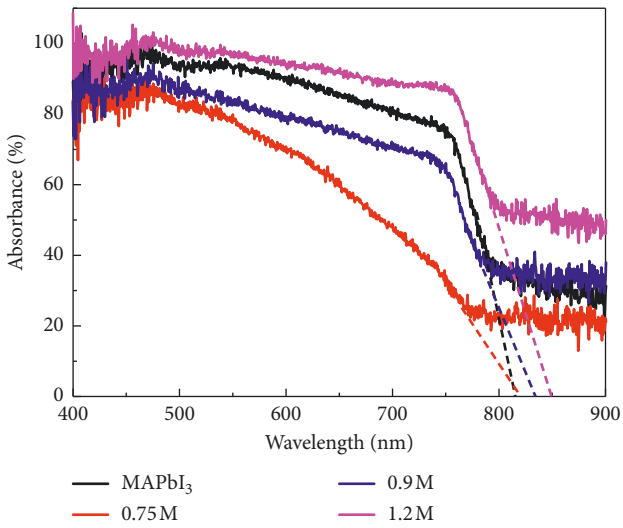

Figure 4: UV-visible absorption spectra of perovskite films with Sample+0 M, Sample+0.75 M, Sample+0.9 M, and Sample+1.2 M.

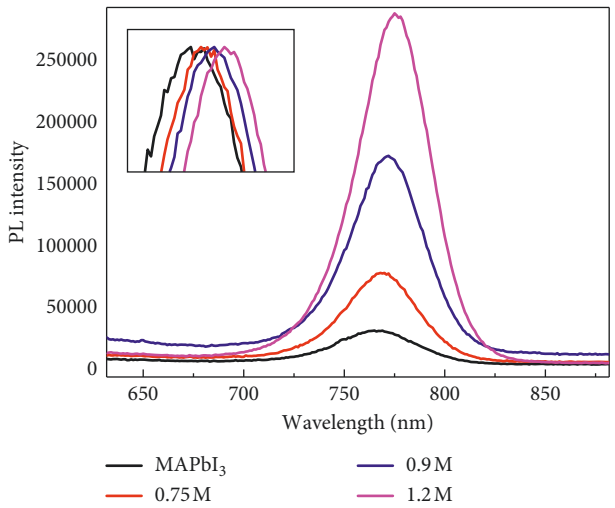

Figure 5: PL spectra of perovskite films with Sample+0 M, Sample+0.75 M, Sample+0.9 M, and Sample+1.2 M.

46.35%, respectively; and the device efficiency is 7.62%, one time greater than that of the PCE of an undoped $MAPbI_3$ perovskite cell device. It can be seen from the above that the device efficiency increases with the increase in the doping concentration of Na^+, while the device efficiency decreases when the doping concentration is Sample+1.2 M. As can be seen from Figure 1, excessive grain boundaries and large cracks were found between the grains of the Sample+1.2 M perovskite layer, resulting in poor contact with the interface of the electron transport layer.

4. Conclusions

According to the above data analysis, perovskite doped with appropriate amount of Na^+ can improve the quality of thin films (including grain size, the effective thickness of the film, surface flatness, and the number of grain boundary, holes, and cracks), and photophysical properties

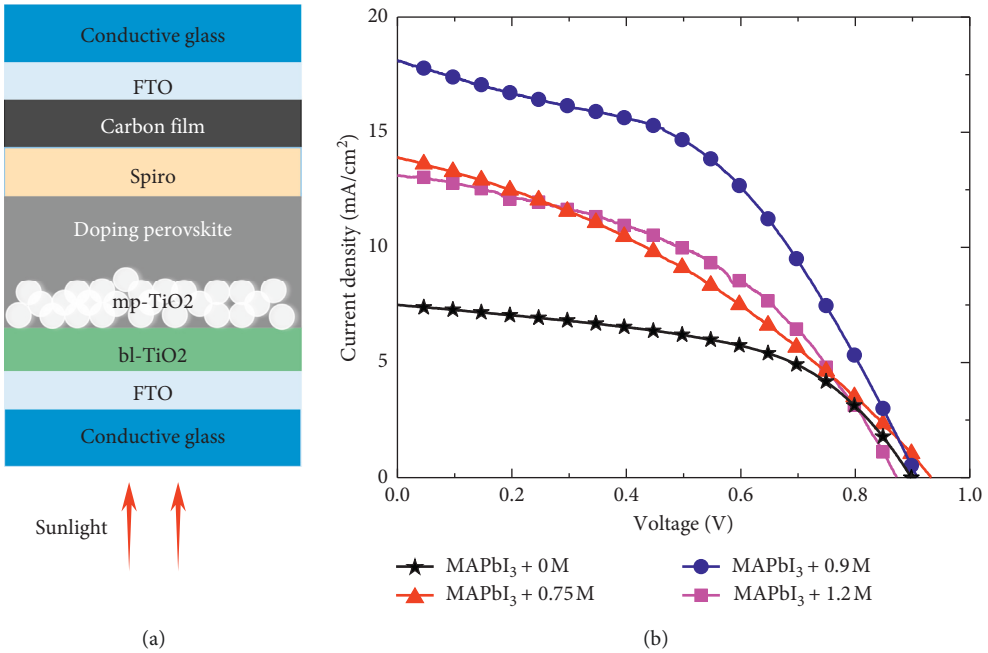

Figure 6: (a) Device structure diagram. (b) Photocurrent voltage density reverse scan (RS) curve of Sample+0 M, Sample+0.75 M, Sample+0.9 M, and Sample+1.2 M.

Table 1: Detailed parameters for reverse scanning of Sample+0 M, Sample+0.75 M, Sample+0.9 M, and Sample+1.2 M.

Samp[1]	J_{sc}[2] (mA/cm^2)	V_{oc}[3] (mV)	FF[4] (%)	PCE[5] (%)
Sample+0 M	7.50	897	52.00	3.49
Sample+0.75 M	13.91	933	35.35	4.59
Sample+0.9 M	18.11	908	46.35	7.62
Sample+1.2 M	13.11	872	44.93	5.14

1, Na^+-doped samples; 2, short-circuit photocurrent density; 3, open-circuit voltage; 4, fill factor; 5, power conversion efficiency.

(including PL launch peak wavelength, PL launch peak displacement, wavelength absorption band displacement, and energy gap change) have a significant impact. In this experiment, the doped perovskite film particles with a concentration of 0.9 mol/L were larger and had better crystallinity. It can be seen from the UV-visible absorption spectrum that its absorption characteristics become better, and the absorption spectrum and PL spectrum are red-shifted compared to pure $MAPbI_3$. EDS also proved that Na^+ was doped into the perovskite absorption layer. This indicates that J_{sc}, PCE, and optical absorption values of the cell devices have been improved within a certain doping range. The experimental samples in this experiment were battery devices with an area of 0.12 cm^2 prepared in air. The carbon film was used as the electrode, and the PCE of the experiment reached 7.62%. It can be seen that the doping process we use is promising and can produce cost-effective devices with low cost in air.

Data Availability

The data used to support the findings of this study are available from the corresponding author upon request.

Conflicts of Interest

The authors declare no conflicts of interest.

Authors' Contributions

C. C. wrote the paper. Y. Y. designed the experiments. C. C. and J. C. analyzed the data. T. L. prepared the samples. H. R. and Y. J. Y. performed all the measurements. X. Z. supervised the project. All authors commented and approved the paper.

Acknowledgments

This research was funded by the project of the Natural Science Foundation of China (no. 61875186), the project of the Natural Science Foundation of Beijing (no. Z160002), the open fund of the State Key Laboratory on Integrated Optoelectronics (no. IOSKL2016KF19), the Key Research Projects of BISTU (2018-22, 2019-22, 2019-23, and 2019-27), and the Beijing Key Laboratory for Sensors of BISTU (no. KF20181077203).

References

[1] N.-G. Park, "Organometal perovskite light absorbers toward a 20% efficiency low-cost solid-state mesoscopic solar cell," *Journal of Physical Chemistry Letters*, vol. 4, no. 15, pp. 2423–2429, 2013.

[2] Y. Guo, C. Liu, K. Inoue, K. Harano, H. Tanaka, and E. Nakamura, "Enhancement in the efficiency of an organic-inorganic hybrid solar cell with a doped P3HT hole-transporting layer on a void-free perovskite active layer," *Journal of Materials Chemistry A*, vol. 2, no. 34, pp. 13827–13830, 2014.

[3] J.-H. Im, I.-H. Jang, N. Pellet, M. Grätzel, and N.-G. Park, "Growth of $CH_3NH_3PbI_3$ cuboids with controlled size for high-efficiency perovskite solar cells," *Nature Nanotechnology*, vol. 9, no. 11, pp. 927–932, 2014.

[4] N. Ahn, D. Y. Son, I. H. Jang et al., "Highly reproducible perovskite solar cells with average efficiency of 18.3% and best efficiency of 19.7% fabricated via Lewis base adduct of lead(II) iodide," *Journal of the American Chemical Society*, vol. 137, no. 27, pp. 8696–8699, 2015.

[5] F. Giordano, A. Abate, J. P. C. Baena et al., "Enhanced electronic properties in mesoporous TiO_2 via lithium doping for high-efficiency perovskite solar cells," *Nature Communications*, vol. 7, article 10379, 2016.

[6] X. Zhang, X. Ren, B. Liu et al., "Stable high efficiency two-dimensional perovskite solar cells via cesium doping," *Energy & Environmental Science*, vol. 10, no. 10, pp. 2095–2102, 2017.

[7] Z. Tang, S. Uchida, T. Bessho et al., "Modulations of various alkali metal cations on organometal halide perovskites and their influence on photovoltaic performance," *Nano Energy*, vol. 45, pp. 184–192, 2018.

[8] D. Bi, A. M. El-Zohry, A. Hagfeldt, and G. Boschloo, "Improved morphology control using a modified two-step method for efficient perovskite solar cells," *ACS Applied Materials & Interfaces*, vol. 6, no. 21, pp. 18751–18757, 2014.

[9] W. Li, J. Fan, J. Li, Y. Mai, and L. Wang, "Controllable grain morphology of perovskite absorber film by molecular self-assembly toward efficient solar cell exceeding 17%," *Journal of the American Chemical Society*, vol. 137, no. 32, pp. 10399–10405, 2015.

[10] T. Salim, S. Sun, Y. Abe, A. Krishna, A. C. Grimsdale, and Y. M. Lam, "Perovskite-based solar cells: impact of morphology and device architecture on device performance," *Journal of Materials Chemistry A*, vol. 3, no. 17, pp. 8943–8969, 2015.

[11] M. K. Kim, H. S. Lee, S. R. Pae et al., "Effects of temperature and coating speed on the morphology of solution-sheared halide perovskite thin-film," *Journal of Materials Chemistry A*, vol. 6, p. 48, 2018.

[12] M. M. Uz Zaman, M. Imran, A. Saleem et al., "Potassium doped methylammonium lead iodide ($MAPbI_3$) thin films as a potential absorber for perovskite solar cells; structural, morphological, electronic and optoelectric properties," *Physica B: Condensed Matter*, vol. 522, pp. 57–65, 2017.

[13] S. Pathak, A. Sepe, A. Sadhanala et al., "Atmospheric influence upon crystallization and electronic disorder and its impact on the photophysical properties of organic-inorganic perovskite solar cells," *ACS Nano*, vol. 9, no. 3, pp. 2311–2320, 2015.

[14] D. J. Freppon, L. Men, S. J. Burkhow, J. W. Petrich, J. Vela, and E. A. Smith, "Photophysical properties of wavelength-tunable methylammonium lead halide perovskite nanocrystals," *Journal of Materials Chemistry C*, vol. 5, no. 1, pp. 118–126, 2017.

[15] B. N. Sara, L. Binbin, A. Ghada et al., "Photophysical properties and improved stability of organic-inorganic perovskite by surface passivation," *Journal of Physical Chemistry C*, vol. 122, no. 28, pp. 15799–15818, 2018.

[16] T. J. Jacobsson, S. Svanström, V. Andrei et al., "Extending the compositional space of mixed lead halide perovskites by Cs, Rb, K, and Na doping," *Journal of Physical Chemistry C*, vol. 122, no. 25, pp. 13548–13557, 2018.

[17] K. Granath, M. Bodegård, and L. Stolt, "The effect of NaF on Cu(In, Ga)Se2 thin film solar cells," *Solar Energy Materials and Solar Cells*, vol. 60, no. 3, pp. 279–293, 2000.

[18] R. Caballero, C. A. Kaufmann, T. Eisenbarth et al., "The influence of Na on low temperature growth of CIGS thin film solar cells on polyimide substrates," *Thin Solid Films*, vol. 517, no. 7, pp. 2187–2190, 2009.

[19] Z.-K. Yuan, S. Chen, Y. Xie et al., "Na-diffusion enhanced p-type conductivity in Cu(In,Ga)Se2: a new mechanism for efficient doping in semiconductors," *Advanced Energy Materials*, vol. 6, no. 24, article 1601191, 2016.

[20] M. Saliba, T. Matsui, K. Domanski et al., "Incorporation of rubidium cations into perovskite solar cells improves photovoltaic performance," *Science*, vol. 354, no. 6309, pp. 206–209, 2016.

[21] M. Saliba, T. Matsui, J.-Y. Seo et al., "Cesium-containing triple cation perovskite solar cells: improved stability, reproducibility and high efficiency," *Energy & Environmental Science*, vol. 9, no. 6, pp. 1989–1997, 2016.

[22] J. Kim, S.-H. Lee, J. H. Lee, and K.-H. Hong, "The role of intrinsic defects in methylammonium lead iodide perovskite," *Journal of Physical Chemistry Letters*, vol. 5, no. 8, pp. 1312–1317, 2014.

[23] W.-J. Yin, T. Shi, and Y. Yan, "Unique properties of halide perovskites as possible origins of the superior solar cell performance," *Advanced Materials*, vol. 26, no. 27, pp. 4653–4658, 2014.

[24] M. Abdi-Jalebi, M. I. Dar, A. Sadhanala et al., "Impact of monovalent cation halide additives on the structural and optoelectronic properties of $CH_3NH_3PbI_3$Perovskite," *Advanced Energy Materials*, vol. 6, no. 10, article 1502472, 2016.

[25] A. Kojima, K. Teshima, Y. Shirai, and T. Miyasaka, "Organometal halide perovskites as visible-light sensitizers for photovoltaic cells," *Journal of the American Chemical Society*, vol. 131, no. 17, pp. 6050-6051, 2009.

[26] W. S. Yang, B.-W. Park, E. H. Jung et al., "Iodide management in formamidinium-lead-halide-based perovskite layers for efficient solar cells," *Science*, vol. 356, no. 6345, pp. 1376–1379, 2017.

[27] A. Mei, X. Li, L. Liu et al., "A hole-conductor-free, fully printable mesoscopic perovskite solar cell with high stability," *Science*, vol. 345, no. 6194, pp. 295–298, 2014.

[28] Y. Yang, X. Zou, Y. Pei, X. Bai, W. Jin, and D. Chen, "Effect of doping of NaI monovalent cation halide on the structural, morphological, optical and optoelectronic properties of $MAPbI_3$ perovskite," *Journal of Materials Science: Materials in Electronics*, vol. 29, no. 1, pp. 205–210, 2018.

[29] N. Zhang, Y. Guo, X. Yin, M. He, and X. Zou, "Spongy carbon film deposited on a separated substrate as counter electrode for perovskite-based solar cell," *Materials Letters*, vol. 182, pp. 248–252, 2016.

[30] T. Ling, X. Zou, J. Cheng, Y. Yang, H. Ren, and D. Chen, "Modulating surface morphology related to crystallization speed of perovskite grain and semiconductor properties of optical absorber layer under controlled doping of potassium ions for solar cells," *Materials*, vol. 11, no. 9, p. 1605, 2018.

[31] T. Ling, X. Zou, J. Cheng, X. Bai, H. Ren, and D. Chen, "Modified sequential deposition route through localized-liquid-liquid-diffusion for improved perovskite multi-crystalline thin films with micrometer-scaled grains for solar cells," *Nanomaterials*, vol. 8, no. 6, p. 416, 2018.

[32] L. Yang, Y. Gao, Y. Wu et al., "Novel insight into the role of chlorobenzene antisolvent engineering for highly efficient perovskite solar cells: gradient diluted chlorine doping," *ACS Applied Materials & Interfaces*, vol. 11, no. 1, pp. 792–801, 2019.

[33] A. M. A. Leguy, Y. Hu, M. Campoy-Quiles et al., "Reversible hydration of $CH_3NH_3PbI_3$ in films, single crystals, and solar cells," *Chemistry of Materials*, vol. 27, no. 9, pp. 3397–3407, 2015.

[34] J. Chang, Z. Lin, H. Zhu et al., "Enhancing the photovoltaic performance of planar heterojunction perovskite solar cells by doping the perovskite layer with alkali metal ions," *Journal of Materials Chemistry A*, vol. 4, no. 42, pp. 16546–16552, 2016.

[35] Z. Tang, T. Bessho, F. Awai et al., "Hysteresis-free perovskite solar cells made of potassium-doped organometal halide perovskite," *Scientific Reports*, vol. 7, no. 1, p. 12183, 2017.